HHS Public Access

Author manuscript

Biomaterials. Author manuscript; available in PMC 2017 April 01.

Published in final edited form as:

Biomaterials. 2016 April ; 86: 1–10. doi:10.1016/j.biomaterials.2016.01.062.

Spatiotemporal Control of Cardiac Anisotropy Using Dynamic Nanotopographic Cues

Paulos Y. Mengsteab[1,‡,†], **Koichiro Uto**[1,2,‡], **Alec S.T. Smith**[1], **Sam Frankel**[1], **Elliot Fisher**[1], **Zeid Nawas**[1], **Jesse Macadangdang**[1], **Mitsuhiro Ebara**[2], and **Deok-Ho Kim**[1,3,4,*]

[1]Department of Bioengineering, University of Washington, Seattle, WA, 98195, USA

[2]International Center for Materials Nanoarchitectonics (WPI-MANA), National Institute for Materials Science (NIMS), 1-1 Namiki, Tsukuba, Ibaraki 305-0044, Japan

[3]Institute for Stem Cell and Regenerative Medicine, University of Washington, Seattle, WA 98109, USA

[4]Center for Cardiovascular Biology, University of Washington, Seattle, WA 98109, USA

Abstract

Coordinated extracellular matrix spatiotemporal reorganization helps regulate cellular differentiation, maturation, and function *in vivo*, and is therefore vital for the correct formation, maintenance, and healing of complex anatomic structures. In order to evaluate the potential for cultured cells to respond to dynamic changes in their *in vitro* microenvironment, as they do *in vivo*, the collective behavior of primary cardiac muscle cells cultured on nanofabricated substrates with controllable anisotropic topographies was studied. A thermally induced shape memory polymer (SMP) was employed to assess the effects of a 90° transition in substrate pattern orientation on the contractile direction and structural organization of cardiomyocyte sheets. Cardiomyocyte sheets cultured on SMPs exhibited anisotropic contractions before shape transition. 48 hours after heat-induced shape transition, the direction of cardiomyocyte contraction reoriented significantly and exhibited a bimodal distribution, with peaks at ~ 45 and −45 degrees ($P < 0.001$). Immunocytochemical analysis highlighted the significant structural changes that the cells underwent in response to the shift in underlying topography. The presented results demonstrate that initial anisotropic nanotopographic cues do not permanently determine the organizational fate or contractile properties of cardiomyocytes in culture. Given the importance of surface cues in regulating primary and stem cell development, investigation of such tunable nanotopographies may have important implications for advancing cellular maturation and

*CORRESPONDING AUTHOR. Prof. Deok-Ho Kim, University of Washington, Department of Bioengineering, N410G William H Foege Building, 3720 15th Ave NE, Box 355061, Seattle, WA 98195, Phone: 1-206-616-1133, Fax: 1-206-685-3300, deokho@uw.edu.

‡Authors contributed equally to this work.

†Present Address

Institute for Regenerative Engineering, University of Connecticut Health, Farmington, CT, 06030, USA.

performance *in vitro*, as well as improving our understanding of cellular development in response to dynamic biophysical cues.

Keywords

Shape memory polymers; nanotopography; ECM; cardiomyocyte; contractile anisotropy

INTRODUCTION

The human extracellular matrix (ECM) is composed of a myriad of protein polymers, signaling molecules, proteases, and growth factors that are specifically tailored, in terms of architecture and composition, to every organ in the body and have pivotal roles in the correct remodeling of each tissue [1]. The ECM forms a dynamic microenvironment that promotes temporal changes in tissue structure to help regulate key cell functions and mechanisms [2, 3]. During embryogenesis, the ECM is particularly important because the spatiotemporal regulation of cell migration, reorganization, and differentiation must be finely coordinated to enable the formation of complex anatomic structures [4]. During heart development specifically, ECM signaling and structural cues play a pivotal role in promoting the development of structural and functional anisotropy, which are critical for enabling effective blood ejection from the ventricles. Given the close association between structural signaling and cardiac physiological function, *in vitro* studies of the mechanisms that underpin cardiomyocyte maturation and performance would greatly benefit from the development of culture environments that more closely recapitulate the dynamic nature of the cardiac microenvironment.

The ability for substrate nanotopography to control cellular and multicellular form and function *in vitro* has been widely investigated [5–11]. In particular, cardiomyocytes are known to develop highly organized and aligned cardiac cell sheets when cultured on anisotropic nanogrooved substrates. In these instances, engineered nanotopographical substrates are designed to mimic the architecture of the native myocardial ECM, which is comprised of highly aligned collagen fiber bundles with an average diameter of 120 – 150 nm [6]. Other engineered platforms have been designed to investigate the effect of the local density of ECM nanotopographic cues on cellular function, and have shown preferential cell migration towards an optimal topographic density [8,12,13]. While these engineered substrates are able to recapitulate the static architecture of the native myocardium or variations in topography, they do little to recreate the dynamic reorganization events that are known to occur throughout the developmental process [14,15]. With recent advances in smart biomaterials, it is now possible to design and fabricate cell culture substrates with dynamic nanoscale topographies to investigate the ability of changing substrate cues to influence cellular development [5].

Shape memory polymers (SMPs), a division of smart biomaterials, are capable of dynamic shape or surface topography transitions as induced by a range of external stimuli. These stimuli include photo irradiation, electromagnetism, pH, and temperature [16–23]. SMPs have been used to demonstrate that a cell loses its cytoskeletal structure in response to

degradation of the underlying substrate topography [24–26]. For example, Davis *et al.* demonstrated that C3H/10T1/2 mouse embryonic fibroblasts cultured on a micropatterned topography aligned with the pattern direction. However, upon shape transition to an unpatterned flat substrate the cells devolved to random alignments [26]. While studies such as these provide interesting observations of dynamic cellular responses to topographic changes, they have so far relied exclusively on microscale topographies, which do not accurately mimic native ECM cues [8]. These studies have also only interrogated alignment at the single-cell level, which neglects tissue level organization and cell-cell cross-talk. Additionally, they have not characterized cellular functionality, which is an important phenotypic indicator of cellular development. Furthermore, these studies assessed the response of motile cells to changes in surface topographies, and therefore did not investigate cellular repolarization. Dynamic regulation of functional cellular characteristics using SMP cell culture platforms on the nanoscale remains an important advancement in the field of smart biomaterials as it enables more accurate modeling of the cell's dynamic extracellular physical environment. Analysis of confluent cell sheets and direct measurement of functional performance on these novel surfaces are of particular importance for cardiac bioengineering as they are necessary for accurately recapitulating native tissue development.

In this study we investigated the role of dynamic anisotropic nanogrooves in regulating the cytoskeletal and focal adhesion alignment as well as contractile function of primary cardiac muscle cells in monolayers. A thermally induced poly(ε-caprolactone) (PCL) SMP with anisotropic nanotopography was engineered to transition its orientation by 90 degrees when exposed to a change in temperature (from here on termed shape transition). The nanoscale cues employed in these experiments were designed to recapitulate the size and orientation of collagen fiber bundles present within the native ECM of human myocardial tissue [6]. The transition temperature of the PCL substrate was tuned to 33°C, which enabled shape transition to occur at a biologically suitable temperature [27]. Using this platform, the effect of temporal changes in anisotropic nanotopography on the collective contraction orientation of primary cardiac muscle cells was assessed.

MATERIALS AND METHODS

Fabrication of cross-linked PCL films

The PCL films were prepared by cross-linking tetra-branched PCL with acrylate end-groups in the presence of linear PCL telechelic diacrylates according to a previously reported protocol [27,28]. The average degrees of polymerization of each branch for two- and four-branch PCL were 18 and 10, respectively. The equimolar amounts of PCL macromonomers were then dissolved at 45 weight % in xylene containing 2-fold molar excess benzoyl peroxide (BPO; Sigma-Aldrich, St. Louis, MO, USA) to the end-group of macromonomers. To fabricate a PCL film with permanent topography, the macromonomer solution was dispensed onto a silicon master (400 nm_500 nm_150 nm, ridge width_groove width_depth) with a 0.1 mm thick Teflon spacer and bound by two glass slides (Figure1A and 1Bi.). Thermal polymerization was carried out at 80°C for 4 hours (Figure 1Bii) and the PCL film was then lifted off (Figure 1Biii.). The thermal and mechanical properties of the cross-linked

materials made from 1:1 2b20/4b10 macromonomer solution have been characterized previously [27].

Fabrication of shape memory polymer with orthogonal nanogrooves

For the study of dynamic contractile orientation, a temporary pattern, which was orthogonal to the permanent pattern, was developed. Permanent patterns were used as a control. As seen in Figure 1Biv, the temporary pattern was heated for 2 minutes at 80°C and then placed onto a silicon master mold, with the patterns of the film and mold offset by 90 degrees. Then, the silicon master and polymer were heated again for 2 minutes at 80°C, and then bound together with a pressure of 0.1 MPa (Figure 1Bv.). The system was then cooled for 1 hour at 4°C, and the polymer was then lifted off (Figure 1Bvi.).

Atomic force microscopy (AFM) of shape memory polymer nanotopography

The surface morphologies of cross-linked PCL films were observed by AFM (SPM-9500J3, Shimadzu Co., Kyoto, Japan) with non-contact mode using a Si_3N_4 cantilever (spring constant; 42 N/m, Nano World, Neuchâtel, Switzerland). The sample temperature was controlled using a thermo controller. The cross-linked PCL films were heated and equilibrated at 32°C and 37°C for 1 hour, and AFM measurement was performed to obtain surface topography and height images.

Real-time topographical observation of shape transition using digital holographic microscopy

The time-dependent surface shape-memory transition of cross-linked PCL films was also observed by holographic microscopy (Lyncée tec R2100, Switzerland). Time-dependent observation in response to temperature change was conducted on a microwarm plate (KM-3, Kitazato Supply CO., Ltd, Sizuoka, Japan). The setting temperature of the microwarm plate was increased from 36.5 to 38.0°C in air, and continuous topographical transition at the surface was observed.

Cardiomyocyte cell culture on PCL SMP substrates

Before cell culture, PCL films were sterilized by incubating for 20 minutes in ethanol at 4°C, plasma treating (100 W, 0.05 Torr, and 5 minutes), and UV sterilizing for 1 hour. The films were then incubated overnight with a fibronectin surface treatment at a concentration of 10 μg/cm^2 in Dulbecco's Phosphate Buffered Saline (DPBS) at pH 7.2. Neonatal rat ventricular myocytes (NRVMs) were isolated from 2-day-old Sprague-Dawley rats and seeded at a density of 5×10^5 cells/cm^2. Cultures were maintained for 5 days at 32°C, and the medium was replaced every 2 days. The medium used consisted of the following: DMEM (high-glucose, -sodium pyruvate) (67%), HEPES (17 mM), M199 (17%), Horse Serum (10%), Fetal Bovine Serum (5%), and Pen-Strep (1%). Ara-C (10 μL/mL) was used to eliminate proliferating cells. For the assessment of contractile direction change, cells were transferred to a 37°C incubator at day 5 and maintained until day 7.

Video acquisition and analysis of collective cardiomyocyte contractions

Videos were captured at a magnification of 20× at 15 fps for cardiomyocyte sheets at day 5 before shape transition and 48 hours after shape transition (Nikon Eclipse Ti, Tokyo, Japan). Analysis of cardiomyocyte contractile orientation was conducted using custom-written MATLAB scripts. Data recordings from three samples were analyzed for each group.

Immunofluorescence staining

SMP substrates were submerged in 4% paraformaldehyde for 15 minutes in order to fix cultured cells for immunostaining. Samples were then permeabilized for 5 minutes in a 0.1% Triton X-100 solution diluted in PBS. Following permeabilization, samples were washed twice in PBS and then blocked for 1 hour at room temperature with a blocking solution consisting of 2% goat serum in PBS. During this incubation, the primary antibody solution was prepared. This solution consisted of a mouse monoclonal antibody against vinculin (AbCam) diluted 1 in 200 in PBS containing 1% goat serum. After blocking, samples were incubated in this primary antibody solution overnight at 4°C. The next day, samples were washed 3 times (5 minutes per wash) in PBS. The secondary antibody solution consisted of Alexafluor-568 goat anti-mouse IgG (Life Technologies) diluted 1 in 200 in PBS containing 1% goat serum. Alexafluor-488 conjugated Phalloidin (Life Technologies) was also included in the secondary antibody solution, at a 1 in 200 concentration, in order to visualize actin fibers within the cultured cells. Following the 3 washes, samples were submerged in the secondary antibody solution and incubated at room temperature in a darkened chamber for 1 hour. Samples were then washed 2 times in PBS and mounted on glass slides using a drop of Vecta Shield mounting medium (Vector Labs). The mounting medium contained DAPI to facilitate visualization of cell nuclei. Samples were stored in the dark at 4°C until ready for analysis.

Immunofluorescence confocal microscopy and cell image analysis

All imaging was performed using a Nikon A1R confocal mounted on a Nikon TiE inverted microscope with a 60× oil immersion objective lens and using the associated Nikon software. Nuclei and cell alignment on permanent and SMP substrates before and after shape transition were quantified in ImageJ. The alignment of the pattern was utilized as the reference angle. Subsequently, the major axis of the nucleus and cytoskeleton were determined and the angle between the major axis and the reference angle was measured (n = 3 for the experimental groups). For cell alignment n = 573, 545, and 441 and for nuclei alignment n =821, 587, and 662 for permanent, before shape transition, and after shape transition substrates, respectively. The area and aspect ratio of vinculin was quantified in ImageJ, and the plugin OrientationJ was utilized to obtain the distribution of vinculin orientation [28]. For vinculin area and aspect ratio analysis, n = 2028, 1997, and 1447 for permanent, before shape transition, and after shape transition substrates, respectively. Cytoskeletal alignment was analyzed using a modified, previously published, MATLAB script [29, 30].

Statistical analysis

The t-test statistic was used to estimate the alignment of collective cardiomyocyte contractions on unpatterned and nanogrooved substrates ($\alpha = 0.05$). Significant changes in the contractile direction of cardiomyocyte sheets before and after shape transition were determined using a paired t-test ($\alpha = 0.05$). For nuclei and cytoskeleton alignment, significant changes in kurtosis was determined using a paired t-test, n = 3. For vinculin area and aspect ratio, significant changes were determined by an unpaired t-test.

RESULTS

Fabrication of PCL SMP with nanogrooves

Shape-memory transition between orthogonally-offset temporary and permanent anisotropic nanogrooves was investigated to determine the fidelity of the surface nanotopography in response to temperature change. Figure 2 shows the topography of surface patterns memorized by cross-linked PCL films as observed by AFM in non-contact mode. AFM characterization was conducted by first embossing permanent and temporary anisotropic nanogrooves with dimensions of 400_500_150 nm (ridge width_groove width_depth) into PCL films using the methods described above. AFM measurement of the temporary nanogrooves showed an average dimension of 380 (±18)_503 (±20)_126 (±10) nm (ridge width_groove width_depth) (Figure 2A and B). The PCL film was found to relinquish its temporary surface pattern when heated to 37°C, completely recovering the permanent surface topography (Figure 2A and B). The average dimension of the recovered permanent nanogrooves was measured to be 297 (±24)_367 (±10)_94 (±6) nm (ridge width_groove width_depth). From these results, we could confirm that permanent nanotopography was completely restored after shape transition, since the permanent nanotopography before programming the temporary pattern was measured to be 295 (±10)_387 (±23)_92 (±3) nm (ridge width_groove width_depth) (Figure 3A and B). It is worth noting that the surface dimension recovered from the post-shape-transition permanent pattern was measured to be slightly smaller (~ 75%) than the dimension of the original silicon mold. This is likely due to PCL swelling during polymerization in solvent and subsequent shrinkage during drying.

Dynamic characterization of PCL nanogroove shape transition

AFM results indicated that the transition of the nanotopographic surface was achieved within 60 minutes of heating at 37°C. However, the kinetics of surface transition and topographical change based on the shape-memory activation were still unknown. To address this issue, digital holographic microscopy was employed to obtain 3D dynamic imagery of surface topography during the shape-memory transition. Holographic microscopy is capable of providing quantitative marker-free imaging under usual laboratory conditions [31, 33]. Although the z-axis resolution is sufficiently high to monitor the change of nanoscale transition, the direct observation of nanotopography with 400_500_150 nm (ridge width_groove width_depth) is made difficult by the reliance of holographic microscopy on standard optical microscope magnifications. Due to low resolution in the x and y axes, a microgroove substrate with 1000_2000_150 nm (ridge width_groove width_depth) was fabricated for higher-resolution realtime digital holographic microscopy. Figure 4 illustrates the surface topographical transition as observed by holographic microscopy during shape-

memory activation, beginning at 36.5°C (t = 0s) and ending at 38°C (t = 131s). Before inducing shape-memory activation, temporary microgrooves on cross-linked PCL were clearly observed (Figure 4A and B (t = 0s)). During heating, the microgrooves gradually changed and became disrupted. Interestingly, two different patterns coexisted as an intermediate surface structure during the transition (Figure 4A and B middle (t = 74 s)). After heating, groove direction was observed to transition 90 degrees from its initial temporary orientation within 131 seconds (Figure 4A and B right (t = 131 s), and Supplementary Video 1). The cross-sectional profiles of the microgrooved surface at the same location are shown in Figure 4C. Since holographic microscopy is not as precise as AFM, it is difficult to estimate the exact pattern size achieved, however, a continuous change of surface morphology was clearly observed during shape transition. While the structure of the x-axis temporary microgrooves deteriorated with time (as shown in Figure 4B and C), permanent microgrooves could be seen developing in the direction of the y-axis, which validated the orthogonal shape transition. The surface topographical transition was relatively fast, completing within several minutes when the sample was heated above T_m.

Analysis of collective cardiomyocyte contractile orientation on unpatterned and nanogrooved PCL substrates

Utilizing the characterized PCL SMP, the role of static and dynamic anisotropic nanotopographical cues on cardiomyocytes contractile direction was investigated. First, whether or not nanotopographic cues on these substrates could initiate anisotropic mechanical contractions in cardiomyocyte sheets was assessed. By tracking the pixel displacement of contracting cardiomyocytes, in captured videos, the average angles of local contractions and their variance was measured. A representative heat map displays the angles of contraction after 5 days of cultivation (Figure 5A and C), which is also presented by quantitative polar plots (Figure 5B and D). The results indicate that on unpatterned substrates the collective contractile direction of cardiomyocytes exhibits a nearly random distribution. In contrast, the nanogrooved substrates were observed to induce anisotropic collective contractions of cardiomyocytes. These findings are further corroborated by an analysis of the distribution of cell orientation on these surfaces (Supplementary Figure 1). Upon analysis of angular distribution, the unpatterned substrates had a negative kurtosis (−0.8797), representing a flatter distribution, whereas nanogrooved substrates had a positive kurtosis (1.374), representing a distribution more peaked than a Gaussian distribution. Finally, a significant difference in angle variation between unpatterned and nanogrooved substrates was detected ($p < 0.001$, F-test statistic). This result can be attributed to the cardiomyocytes' detection of structural cues imparted by anisotropic nanoscale topographies on patterned substrates, and detection of no such mechanical cues on unpatterned substrates.

Reorganization of cardiomyocytes alignment and contractile direction on nanogrooved PCL shape memory polymer

Analysis of static substrates clearly demonstrated that surface topographical cues influence the contractile direction of cardiomyocyte sheets, which is in line with previously published results [6,8]. However, it was still unknown whether dynamic nanotopographic cues have a causal or determinate effect on the direction of cardiomyocyte anisotropic contractions. To assess this, the PCL SMP platform, as described above, was employed. Before shape

transition, cardiomyocyte sheets at day 5 exhibited anisotropic contractions (Figure 6A) with a kurtosis of 2.184 and a mean angle of −4 degrees. This suggests highly aligned mechanical contractions of the cardiomyocyte sheets influenced by the underlying anisotropic nanotopographical cue. At day 5, the temperature was increased from 32 °C to 37 °C, which is the narrowest temperature range published to induce a shape transition. At day 7, the angle distribution of cardiomyocyte collective contractions was assessed, and it was found that after shape transition the contractions of the cardiac cell sheets shifted orientation by 45 degrees in a bimodal manner and a kurtosis of −1.220 (Figure 6B). Furthermore, it was found that the change in topography induced a significant change in angle distribution (Figure 6C, $p < 0.0001$, paired t-test). The shifting of contraction direction angle demonstrated a bimodal distribution with peaks at ~ 45 and −45 degrees was less than the directional change of the surface topography (90 degrees). Nevertheless, these results clearly suggested that angle distribution of cardiomyocyte collective contractions were dynamically regulated by the change in underlying substrate topography.

Reorganization of cardiomyocyte nuclear and cell alignment on nanogrooved PCL shape memory polymer

It would follow that a change in cardiomyocyte contractile direction would correspond with an alteration in cardiomyocyte alignment. Therefore, the nuclei and cell alignment on substrates that underwent no shape transition and shape transition were assessed. As was observed during contractile analysis, it was found that cardiomyocytes were well aligned with the nanotopographical cues before shape transition (Figure 6D and F). However, after shape transition the alignment of cardiomyocytes did not coincide with the nanotopographical cues reliably (Figure 6E and F). By quantifying the kurtosis of nuclei alignment (Figure 6F), it was found that before shape transition substrates had a peaked distribution (n = 3, kurtosis = 1.207, respectively). After shape transition, nuclear alignment demonstrated a flatter distribution (kurtosis = −1.379), however a slight bimodal distribution is seen, suggesting that cardiomyocytes were reorienting in two directions

Shape Memory Transition affects Vinculin Size and Orientation

It was hypothesized that a change in substrate orientation would disrupt cardiomyocyte focal adhesion complexes due to the reorganization of adhesion area available underneath cultured cells. Therefore, vinculin structure was investigated on permanent and SMP substrates. Through immunofluorescence staining, it was observed that focal adhesions were uniform in size and orientation on substrates before shape transition (Figure 7A). At day 7 (2 days after shape transition), the overall focal adhesion size was found to diminish significantly (Figure 7B). While focal adhesion clusters were still present after shape transition, their structures exhibited more dispersed orientations when compared with samples fixed before shape transition. Analysis of vinculin orientation on permanent and SMP substrates revealed that shape transition had an effect on the alignment of vinculin structures. On permanent substrates and SMP substrates before shape transition, vinculin orientation aligned well with the underlying anisotropic nanogrooves (Figure 7C and D; kurtosis = 0.031, and 0.45 respectively). Interestingly, after shape transition vinculin orientation exhibited a bimodal distribution (kurtosis = −0.67), with peaks at +40 and −50 degrees, which suggests that focal adhesion complex organization in these cardiomyocytes was disorientated. This bimodal

orientation in SMP cultures after shape transition may be attributable to a subset of cells attempting to realign with the shifted underlying topography by reorienting themselves in a clockwise direction, while another subpopulation turned in a counter-clockwise direction.

In addition to orientation, the size of vinculin structures was assessed. A significant difference in vinculin size was found when cardiomyocytes were cultured on permanent vs SMP substrates (Figure 7F). The significant change in vinculin size between permanent substrates and SMP substrates before shape transition can be attributed to the dimensions of the nanogrooved substrate (larger groove width and ridge width dimensions for temporary patterns). However, after shape transition nanogroove dimensions were equivalent to that of the static substrates, but a significant change in vinculin structure size was still present. In our analysis of vinculin structure aspect ratio. It was found that the temporary substrates had the greatest aspect ratio (2.46 ± 0.91), which was substantially different from permanent substrates and SMP after shape transition (mean = 2.35 ± 0.75, and 2.31 ± 0.7123 respectively). The changes in vinculin cluster area and orientation after shape transition suggests that the shape transition event disrupted focal adhesion complexes in the cultured cardiomyocytes.

DISCUSSION

Shape-memory cell culture substrates have the ability to return from a temporary topographic state to their permanent topography when acted on by an external stimulus. As such, these surfaces have drawn much attention as a new category of dynamic cell culture platforms for fundamental research and practical applications (i.e. cardiovascular stents, mesenchymal stem cell differentiation platforms, cell delivery scaffold for *in vivo* tissue repair, etc.) [24–27,34]. Among them, thermally induced SMPs have been the most extensively investigated. Such SMPs are programmed by mechanically embossing the desired topography into the polymer surface at temperatures which exceed the material's glass transition temperature (T_g) or melting temperature (T_m) [24,26,27]. In general, the use of T_m as the triggering switch is more favorable for rapid and sharp surface transitions because the enthalpy change of a solid-liquid phase transition is much larger than that of a glass-rubber transition [35,36]. Ebara *et al.* recently developed a thermally induced SMP using cross-linked PCL, which has an adjustable T_m near biologically relevant temperatures. The T_m of PCL was modulated by adjusting elements of the molecular nano-architectures of component macromonomers including the number of branched arms and molecular weight [32]. A previous study showed that the strain fixity rate R_f and the strain recovery rate R_r in cross-linked PCL were approximately 99% and 90%, respectively [27]. In general, R_f and R_r values lower as T_m decreases because the enthalpy observed around T_m, which corresponds to degree of crystallization, is reduced by hindering crystallization of polymer chains. However, results indicate that cross-linked PCL has excellent bulk and surface material with shape-memory ability.

A previous study utilizing PCL SMPs demonstrated the ability of NIH/3T3 cells to reorganize their cytoskeletons within 24 – 48 hours after shape transition [27]. In addition, the study demonstrated high cell viability at the 32°C culture temperature for NIH/3T3 fibroblasts and C2C12 myoblasts on PCL SMPs [27,37]. These investigations focused on

single cell behavior. Therefore, it was expected that the contractile direction of cardiomyocyte sheets would change in harmony with the shift in nanotopography. Furthermore, to maintain a pure cardiomyocyte culture, the medium was supplemented with Cytarabine (Ara-C) to inhibit fibroblast proliferation, allowing for cardiomyocyte repolarization without an increase in cellular density.

In this study, the collective contractile direction of cardiac cell sheets after shape transition exhibited an affinity to the change in nanotopography orientation. However, a discrepancy between nanotopography and contractile direction was seen. Interestingly, the observed bimodal distribution at ~ 45 and −45 degrees coincides with the vector sum of anisotropic nanotopography before and after shape transition. This was corroborated by examining the nuclear and cytoskeleton alignment before and after shape transition, which highlights the dispersal in cellular alignment brought about by substrate reorganization. Additionally, vinculin positivity in cardiomyocytes was investigated before and after shape transition to determine the effect of this change in underlying topography on focal adhesion complex structure. An analysis of vinculin aspect ratio showed that shape transition did not affect the elongation of vinculin structures, the elongation profile was similar to the control substrate, suggesting that the focal adhesion complexes had matured at day 7. Previous studies using shape memory polymers have assessed the cytoskeleton alignment of single cells, and shown that cells exhibit the ability to reorient with an orthogonal change in substrate topography [5,24,26,38]. However, it has been noted that high cell densities decrease cell locomotion due to contact inhibition of adjacent cells [39–45]. Unlike single cells, cardiac cell sheets maintained on surfaces that have undergone a transition in topography are exposed to conflicting vector components, which influence the dynamic orientation of contractile direction. In such cultures, new substrate anisotropic cues conflict with extant cardiomyocyte intracellular structural alignment. Consequentially, complete reorganization of cell alignment in response to shape transition is likely to be inhibited by existing cell-cell adhesions, and the limited space for accommodating cellular re-orientation. Finally, the observed bimodal distribution of vinculin structures suggests that the cardiomyocytes re-orient in a clockwise or counterclockwise manner. Therefore, it is likely that cardiac cell sheets attempt to re-orient their focal adhesion complexes, face contact inhibition, and lead to only a partial transition of contractile direction in response to altered nanotopographical cues.

These results demonstrate that dynamic control of anisotropic nanogrooves exerts a dramatic effect on the direction of collective cardiomyocyte contractions as well as reorganization of cellular structural alignment. The collective contractile orientation, not only cell alignment, can be successfully and dynamically regulated using surface shape-memory transition, which has not been explored in previous studies. This is the first report describing the dynamic regulation of collective cell behaviors by manipulating surface topographies *in vitro*. Shape-memory substrates with well-defined topographical features offer the opportunity to investigate dynamic cell or tissue responses to their surrounding topographical environments, and may serve as the basis for further development of spatiotemporal tunable materials to direct cell functions for tissue engineering applications [46–50].

CONCLUSIONS

This work highlights a simply fabricated, shape memory polymer with tunable nanogeometry to control and study the structural and contractile anisotropy of cardiac cell sheets. PCL SMPs displayed a quick shape transition upon heat activation, and reoriented their temporary surface pattern by 90 degrees. Cardiomyocyte sheets' contractile direction aligned well with the nanotopography, and demonstrated an ability to reorganize their contractile direction upon shape transition. These results suggest that nanotopographical cues have a causal effect on cardiomyocyte contractile direction, and that continuous substrate pattern signaling is necessary to maintain structural and functional anisotropy in cultured cardiomyocytes.

Supplementary Material

Refer to Web version on PubMed Central for supplementary material.

Acknowledgments

This work was supported by an American Heart Association (AHA) Scientist Development Grant (13SDG14560076). D. H. Kim thanks the Department of Bioengineering at the University of Washington for the new faculty startup fund. P.Y. Mengsteab was supported by a grant to the University of Washington PREP program from NIH-NIGMS 2R25GM086304. K. Uto is supported by Japan Society for the Promotion of Science (JSPS) Postdoctoral Fellowship for Research Abroad for the present work at University of Washington, USA. A.S.T. Smith is supported by an NIH T32 post-doctoral fellowship (2T32HL007312-36A1)

REFERENCES

1. Spinale FG. Myocardial matrix remodeling and the matrix metalloproteinases: influence on cardiac form and function. Physiol Rev. 2007; 87:1285–1342. [PubMed: 17928585]
2. Kassiri Z, Khokha R. Myocardial extra-cellular matrix and its regulation by metalloproteinases and their inhibitors. J Thromb Haemost. 2005; 93:212–219.
3. Jacot JG, McCulloch AD, Omens JH. Substrate stiffness affects the functional maturation of neonatal rat ventricular myocytes. Biophys J. 2008; 95:3479–3487. [PubMed: 18586852]
4. Lockhart M, Wirrig E, Phelps A, Wessels A. Extracellular matrix and heart development. Birth Defects Res A Clin Mol Teratol. 2011; 91:535–550. [PubMed: 21618406]
5. Kim J, Hayward RC. Mimicking dynamic in vivo environments with stimuli-responsive materials for cell culture. Trends Biotechnol. 2012; 30:426–439. [PubMed: 22658474]
6. Kim D-H, Lipke Ea, Kim P, Cheong R, Thompson S, Delannoy M, et al. Nanoscale cues regulate the structure and function of macroscopic cardiac tissue constructs. Proc Natl Acad Sci U S A. 2010; 107:565–570. [PubMed: 20018748]
7. Kim D-H, Kshitiz Smith RR, Kim P, Ahn EH, Kim HN, et al. Nanopatterned cardiac cell patches promote stem cell niche formation and myocardial regeneration. Integr Biol United Kingdom. 2012; 4:1019–1033.
8. Kim D-H, Provenzano PP, Smith CL, Levchenko A. Matrix nanotopography as a regulator of cell function. J Cell Biol. 2012; 197:351–360. [PubMed: 22547406]
9. Dvir T, Timko BP, Kohane DS, Langer R. Nanotechnological strategies for engineering complex tissues. Nat Nanotechnol. 2011; 6:13–22. [PubMed: 21151110]
10. Wang P-Y, Yu J, Lin J-H, Tsai W-B. Modulation of alignment, elongation and contraction of cardiomyocytes through a combination of nanotopography and rigidity of substrates. Acta Biomater. 2011; 7:3285–3293. [PubMed: 21664306]

11. Kai D, Prabhakaran MP, Jin G, Ramakrishna S. Guided orientation of cardiomyocytes on electrospun aligned nanofibers for cardiac tissue engineering. J Biomed Mater Res B Appl Biomater. 2011; 98:379–386. [PubMed: 21681953]
12. Kim D-H, Han K, Gupta K, Kwon KW, Suh K-Y, Levchenko A. Mechanosensitivity of fibroblast cell shape and movement to anisotropic substratum topography gradients. Biomaterials. 2009; 30:5433–5444. [PubMed: 19595452]
13. Kim D-H, Seo C-H, Han K, Kwon KW, Levchenko A, Suh K-Y. Guided cell migration on microtextured substrates with variable local density and anisotropy. Adv Funct Mater. 2009; 19:1579–1586. [PubMed: 20046799]
14. Cox TR, Erler JT. Remodeling and homeostasis of the extracellular matrix: implications for fibrotic diseases and cancer. Dis Model Mech. 2011; 4:165–178. [PubMed: 21324931]
15. Lu P, Weaver VM, Werb Z. The extracellular matrix: a dynamic niche in cancer progression. J Cell Biol. 2012; 196:395–406. [PubMed: 22351925]
16. Jiang HY, Kelch S, Lendlein A. Polymers move in response to light. Adv Mater. 2006; 18:1471–1475.
17. Lendlein A, Jiang H, Jünger O, Langer R. Light-induced shape-memory polymers. Nature. 2005; 434:879–882. [PubMed: 15829960]
18. Zhang C-S, Ni Q-Q, Fu S-Y, Kurashiki K. Electromagnetic interference shielding effect of nanocomposites with carbon nanotube and shape memory polymer. Compos Sci Technol. 2007; 67:2973–2980.
19. Galaev I. “Smart” polymers and what they could do in biotechnology and medicine. Trends Biotechnol. 1999; 17:335–340. [PubMed: 10407406]
20. Liu C, Qin H, Mather PT. Review of progress in shape-memory polymers. J Mater Chem. 2007; 17:1543.
21. Lendlein A, Kelch S. Shape-memory polymers. Angew Chemie Int Ed. 2002; 41:2034.
22. Behl M, Razzaq MY, Lendlein A. Multifunctional shape-memory polymers. Adv Mater. 2010; 22:3388–3410. [PubMed: 20574951]
23. Mather PT, Luo X, Rousseau IA. Shape memory polymer research. Annu Rev Mater Res. 2009; 39:445–471.
24. Le DM, Kulangara K, Adler AF, Leong KW, Ashby VS. Dynamic topographical control of mesenchymal stem cells by culture on responsive poly(ε-caprolactone) surfaces. Adv Mater. 2011; 23:3278–3283. [PubMed: 21626577]
25. Tseng L-F, Mather PT, Henderson JH. Shape-memory-actuated change in scaffold fiber alignment directs stem cell morphology. Acta Biomater. 2013; 9:8790–8801. [PubMed: 23851156]
26. Davis KA, Burke KA, Mather PT, Henderson JH. Dynamic cell behavior on shape memory polymer substrates. Biomaterials. 2011; 32:2285–2293. [PubMed: 21224032]
27. Ebara M, Uto K, Idota N, Hoffman JM, Aoyagi T. Shape-memory surface with dynamically tunable nano-geometry activated by body heat. Adv Mater. 2012; 24:273–278. [PubMed: 21954058]
28. Rezakhaniha R, Agianniotis A, Schrauwen JTC, Griffa A, Sage D, Bouten CVC, et al. Experimental investigation of collagen waviness and orientation in the arterial adventitia using confocal laser scanning microscopy. Biomech. Model. Mechanobiol. 2012; 11:461–473. [PubMed: 21744269]
29. Chaterji S, Kim P, Choe SH, Tsui JH, Lam CH, Ho DS, et al. Synergistic effects of matrix nanotopography and stiffness on vascular smooth muscle cell function. Tissue Eng. Part A. 2014; 20:2115–2126. [PubMed: 24694244]
30. Cho H, Jönsson H, Campbell K, Melke P, Williams JW, Jedynak B, et al. Self-organization in high-density bacterial colonies: efficient crowd control. PLoS Biol. 2007; 5:e302. [PubMed: 18044986]
31. Ebara M, Akimoto M, Uto K, Shiba K, Yoshikawa G, Aoyagi T. Focus on the interlude between topographic transition and cell response on shape-memory surfaces. Polymer (Guildf). 2014; 55:5961–5968.

32. Uto K, Yamamoto K, Hirase S, Aoyagi T. Temperature-responsive cross-linked poly(epsilon-caprolactone) membrane that functions near body temperature. J Control Release. 2006; 110:408–413. [PubMed: 16332350]
33. Mihailescu M, Popescu RC, Matei A, Acasandrei A, Paun IA, Dinescu M. Investigation of osteoblast cells behavior in polymeric 3D micropatterned scaffolds using digital holographic microscopy. Appl Opt. 2014; 53:4850–4858. [PubMed: 25090313]
34. Small W, Singhal P, Wilson TS, Maitland DJ. Biomedical applications of thermally activated shape memory polymers. J Mater Chem. 2010; 20:3356–3366. [PubMed: 21258605]
35. DiOrio AM, Luo X, Lee KM, Mather PT. A functionally graded shape memory polymer. Soft Matter. 2011; 7:68–74.
36. Xie T. Tunable polymer multi-shape memory effect. Nature. 2010; 464:267–270. [PubMed: 20220846]
37. Uto K, Ebara M, Aoyagi T. Temperature-responsive poly(ε-caprolactone) cell culture platform with dynamically tunable nano-roughness and elasticity for control of myoblast morphology. Int J Mol Sci. 2014; 15:1511–1524. [PubMed: 24451135]
38. Yakacki CM, Shandas R, Safranski D, Ortega AM, Sassaman K, Gall K. Strong, tailored, biocompatible shape-memory polymer networks. Adv Funct Mater. 2008; 18:2428–2435. [PubMed: 19633727]
39. Abercrombie M, Heaysman JEM. Observations on the social behaviour of cells in tissue culture. Exp Cell Res. 1954; 6:293–306. [PubMed: 13173482]
40. Stoker MGP, Rubin H. Density dependent inhibition of cell growth in culture. Nature. 1967; 215:171–172. [PubMed: 6049107]
41. Trepat X, Wasserman MR, Angelini TE, Millet E, Weitz DA, Butler JP, et al. Physical forces during collective cell migration. Nat Phys. 2009; 5:426–430.
42. Ilina O, Friedl P. Mechanisms of collective cell migration at a glance. J Cell Sci. 2009; 122:3203–3208. [PubMed: 19726629]
43. Weijer CJ. Collective cell migration in development. J Cell Sci. 2009; 122:3215–3223. [PubMed: 19726631]
44. Angelini TE, Hannezo E, Trepat X, Marquez M, Fredberg JJ, Weitz DA. Glass-like dynamics of collective cell migration. Proc Natl Acad Sci U S A. 2011; 108:4714–4719. [PubMed: 21321233]
45. Rørth P. Collective cell migration. Annu Rev Cell Dev Biol. 2009; 25:407–429. [PubMed: 19575657]
46. Morrison SJ, Shah NM, Anderson DJ. Regulatory mechanisms in stem cell biology. Cell. 1997; 88:287–298. [PubMed: 9039255]
47. Guilak F, Cohen DM, Estes BT, Gimble JM, Liedtke W, Chen CS. Control of stem cell fate by physical interactions with the extracellular matrix. Cell Stem Cell. 2009; 5:17–26. [PubMed: 19570510]
48. Vogel V, Sheetz MP. Cell fate regulation by coupling mechanical cycles to biochemical signaling pathways. Curr Opin Cell Biol. 2009; 21:38–46. [PubMed: 19217273]
49. Lutolf MP, Hubbell JA. Synthetic biomaterials as instructive extracellular microenvironments for morphogenesis in tissue engineering. Nat Biotechnol. 2005; 23:47–55. [PubMed: 15637621]
50. Lutolf MP, Gilbert PM, Blau HM. Designing materials to direct stem-cell fate. Nature. 2009; 462:433–441. [PubMed: 19940913]

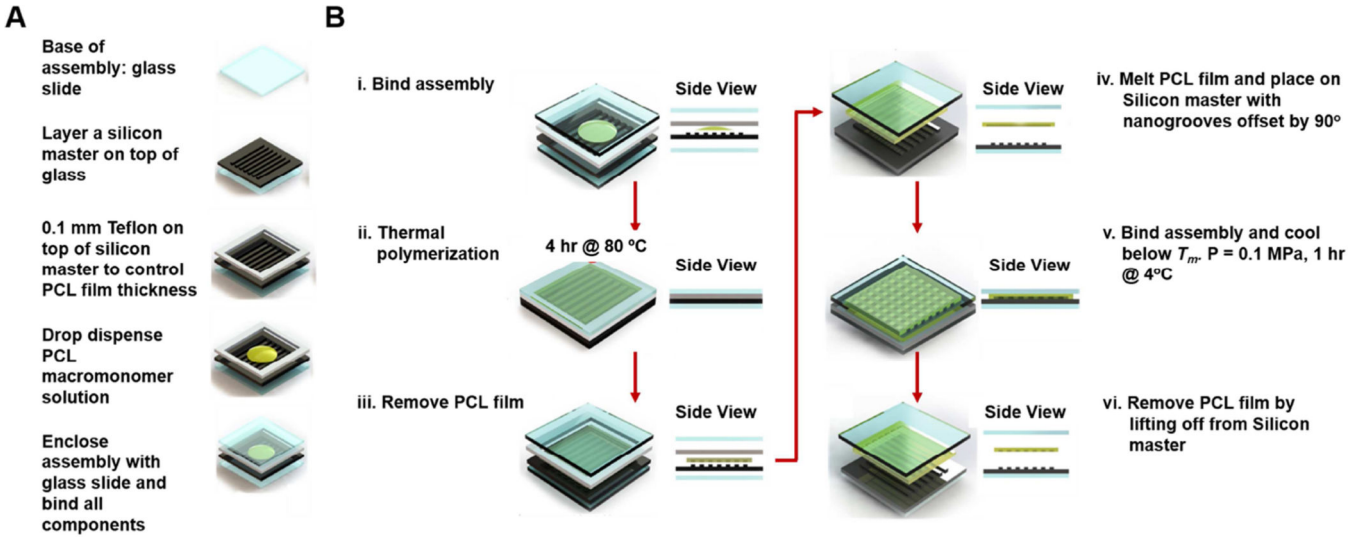

Figure 1. Fabrication of PCL-based shape memory nanogrooves with a temporary and permanent state

(A) During prefabrication assembly, a Teflon spacer is used to control PCL film thickness, and PCL macromonomer solution is sandwiched between a silicon master and glass slides. The assembly is bound (Bi.) and then thermal polymerization takes place at 80°C for 4 hours (Bii.). Then, the PCL film is lifted off with a nanogrooved permanent state (Biii.). Next, a temporary pattern with anisotropic nanogrooves oriented 90 degrees from the permanent state is fabricated. (Biv.) The permanent pattern is melted at 80°C for 2 minutes and then placed on the silicon master with a 90 degree groove offset. It is then bound in between glass slides with a pressure of 0.1 MPa. (Bv.) The assembly is cooled for 1 hour at 4°C, and then the PCL film is lifted off (Bvi.), achieving a PCL-based SMP with a temporary and permanent anisotropic nanogrooved state that are *orthogonally offset*.

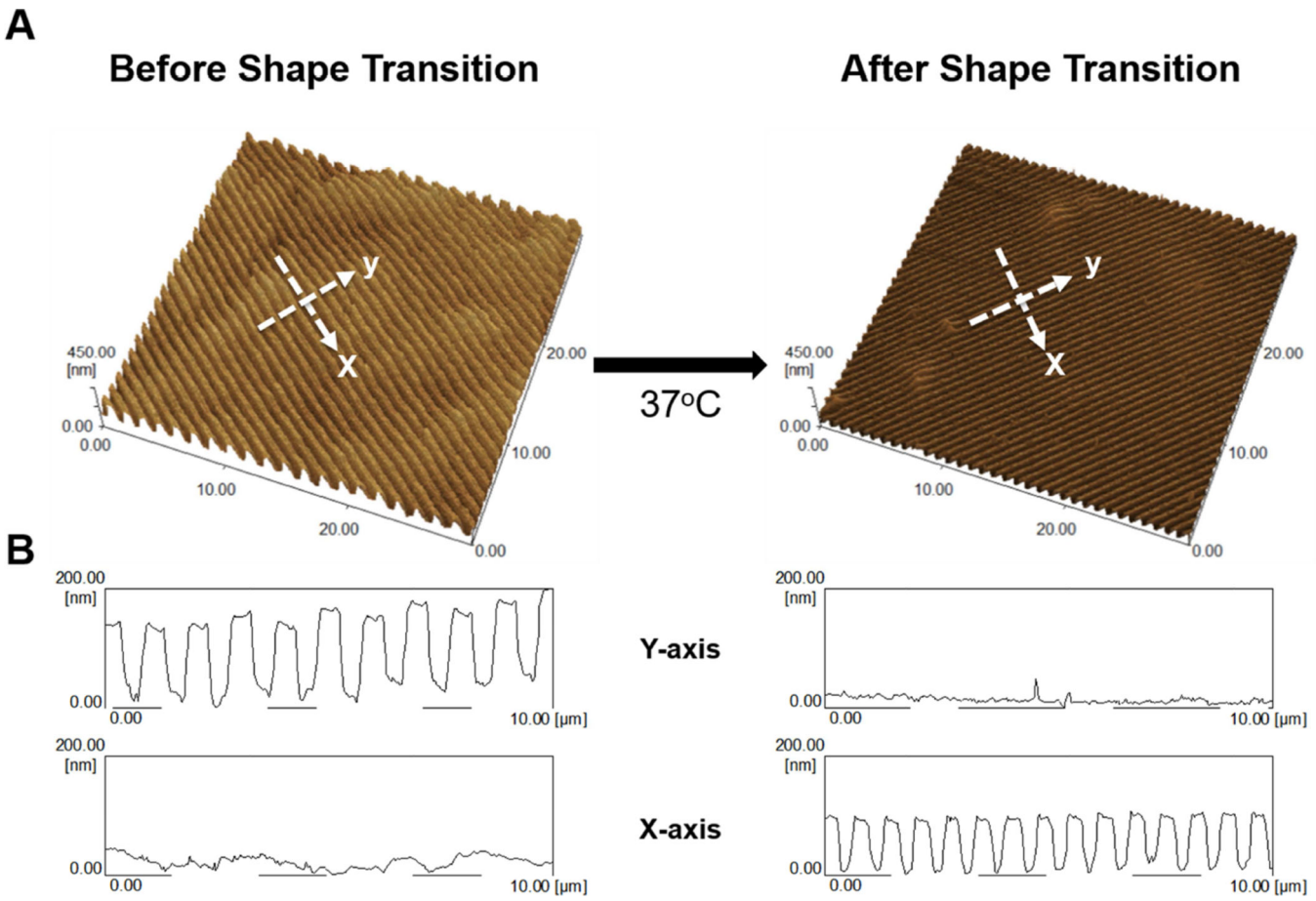

Figure 2. AFM characterization of PCL temporary and permanent topography

(A) Atomic force microscopy image of temporary and permanent topographies after heat-induced shape transition. (B) Cross-sectional profiles of temporary and permanent PCL topography's ridge, groove, and depth in the x- and y-axis direction indicated by arrows in (A).

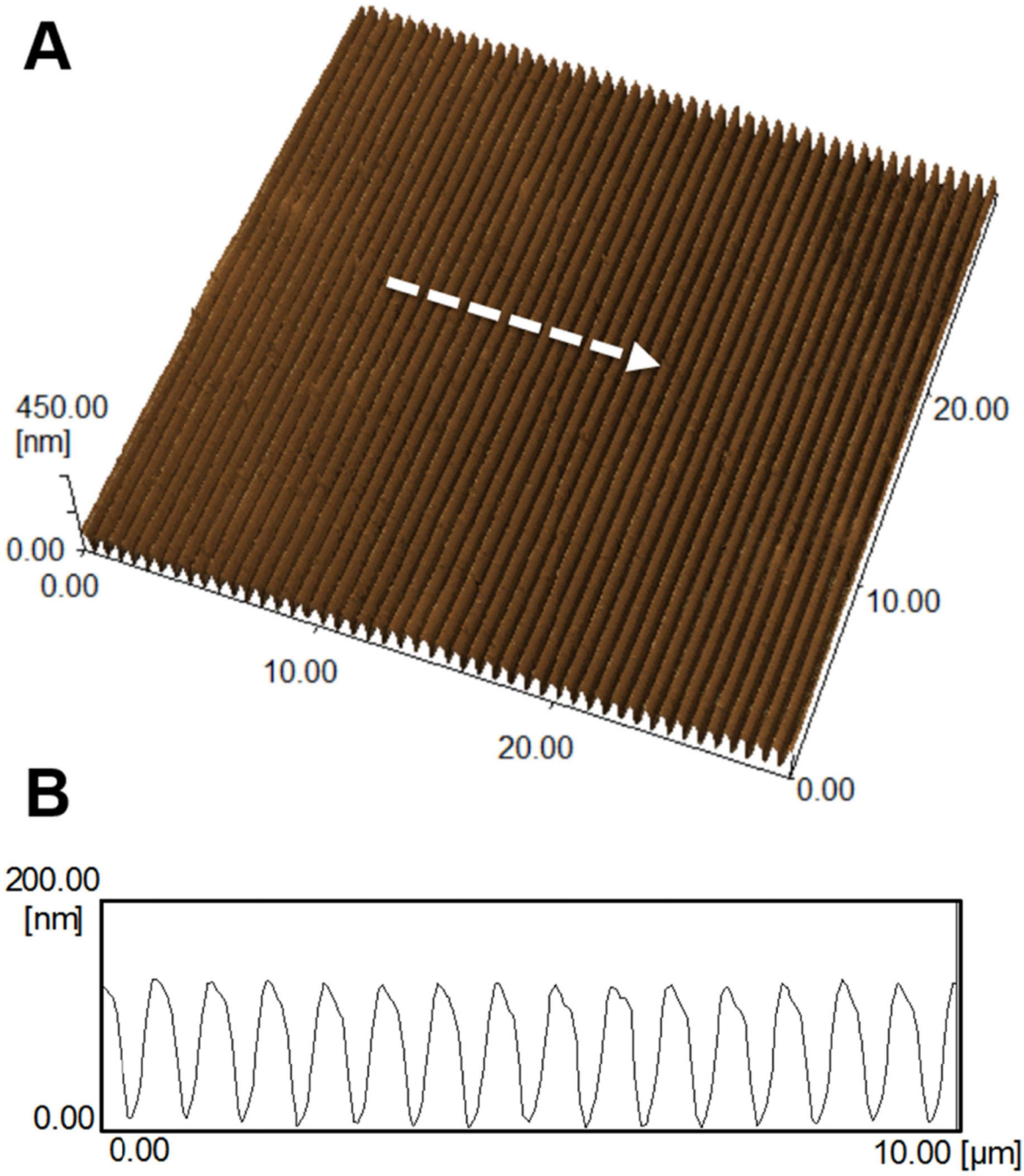

Figure 3. AFM characterization of permanent PCL topography prior to embossing a temporary pattern

(A) Atomic force microscopy image of a permanent PCL topography. (B) Cross-sectional profile of permanent PCL topography's ridge, groove, and depth indicated by arrow in (A).

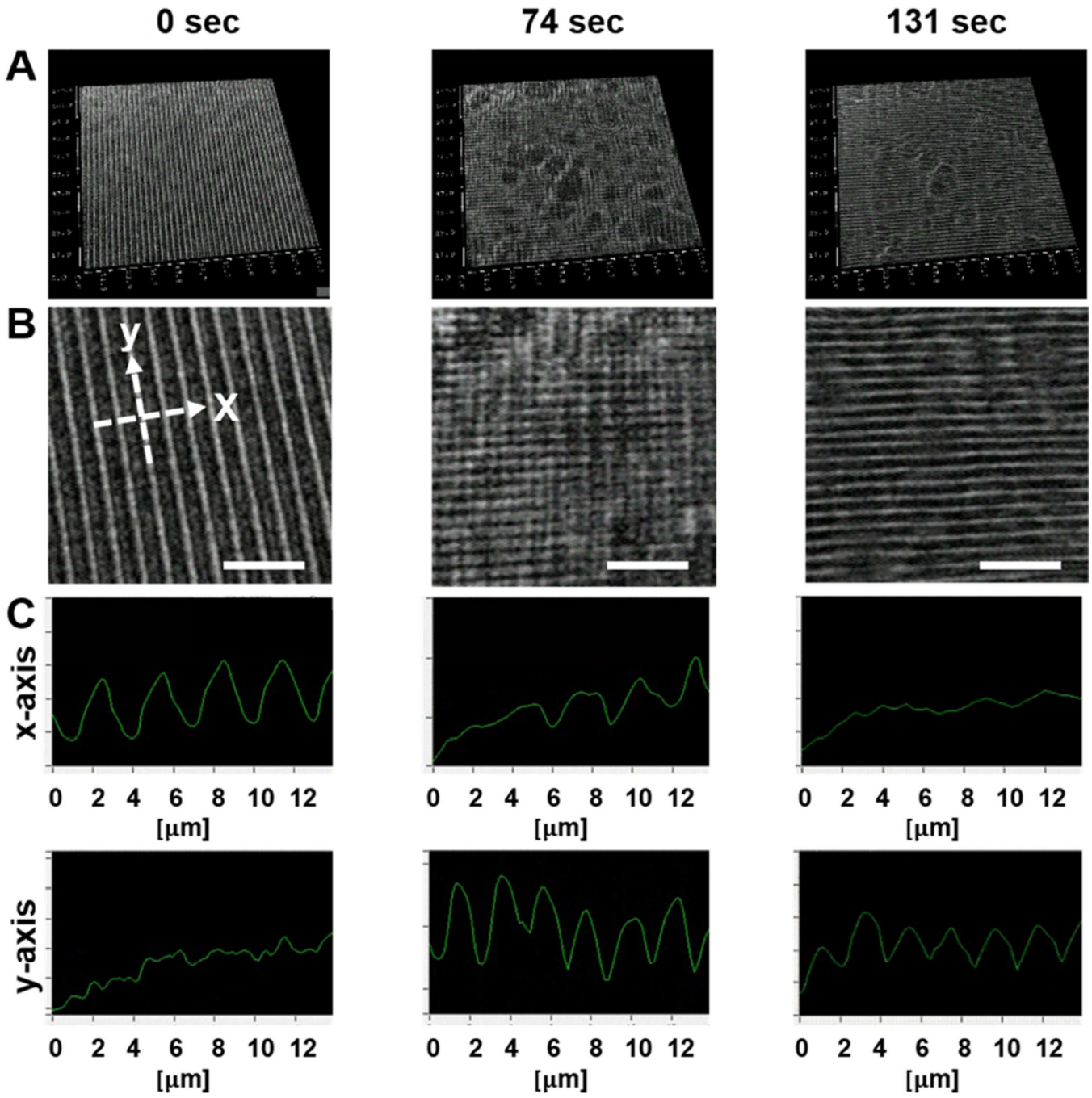

Figure 4. Dynamic holographic microscopy analysis of PCL shape transition

The shape memory polymer's anisotropic topography shifts orientation by 90 degrees during shape transition. (A) Snapshots of PCL topography with 2000_1000_150 nm (groove_ridge_depth) dimensions during shape transition at 0, 74, and 131 seconds. (B) Magnified image of (A) with reference axes for quantifiable analysis of topographic change (scale bar = 10 μm). (C) The x- and y-axis demonstrate the orthogonal pattern shift over time, with deterioration of topography in the x-axis and development of topography in the y-axis. At 131 seconds a clear shift in topography from the x to the y axis is seen.

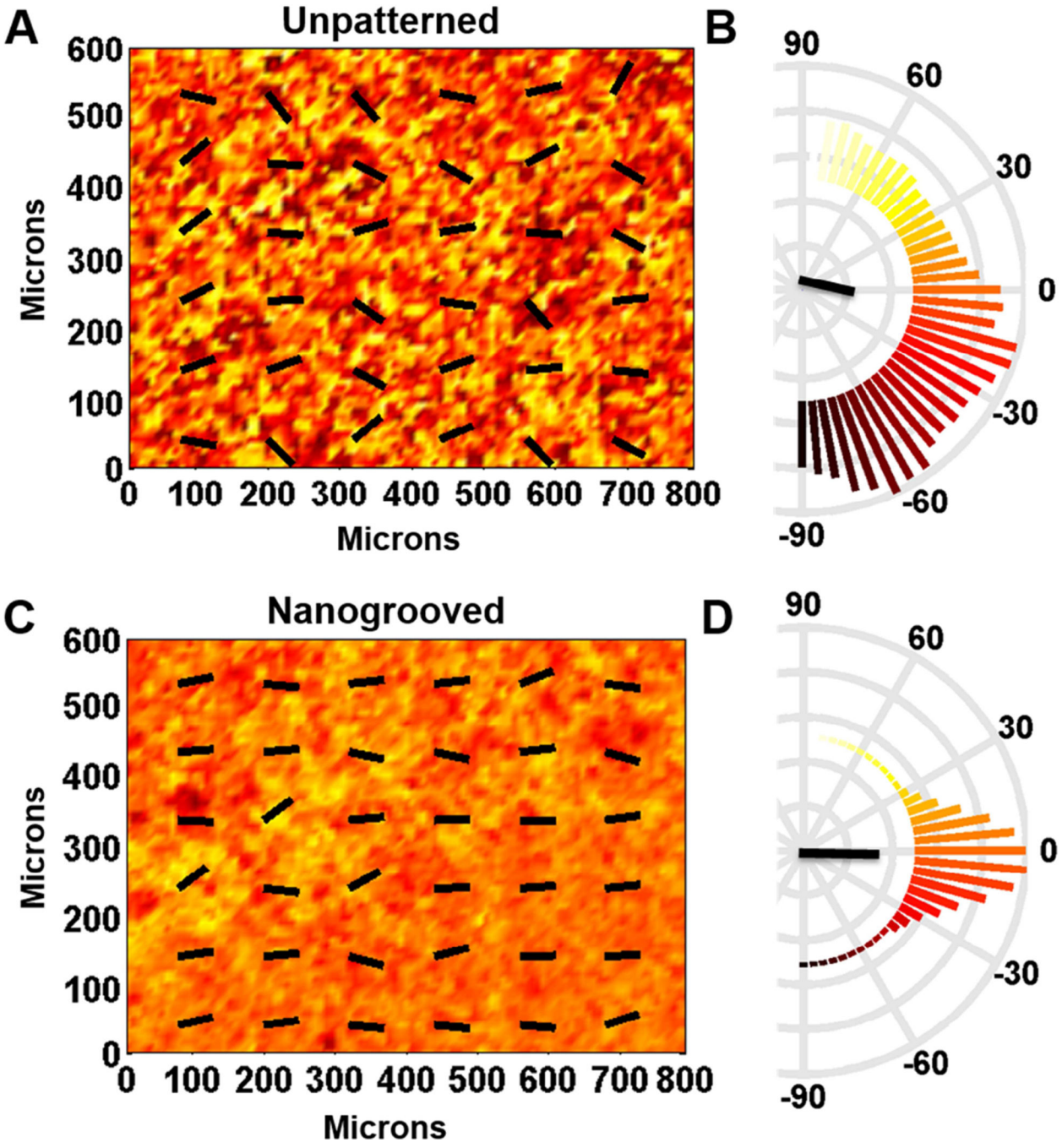

Figure 5. Contraction analysis of cardiac cell monolayer cultured on permanently unpatterned and nanogrooved substrata

The direction of contraction at each location on unpatterned (A) and nanogrooved (C) substrata is indicated by color [coded to the polar histograms in (B) and (D)] and the overlaid vector field. Semicircular histograms of contraction angles indicate the overall directionality of contracting cardiac cells on the unpatterned substratum (B) and the nanogrooved substratum (D). The black lines in the center of the histogram indicate the mean resultant vector length.

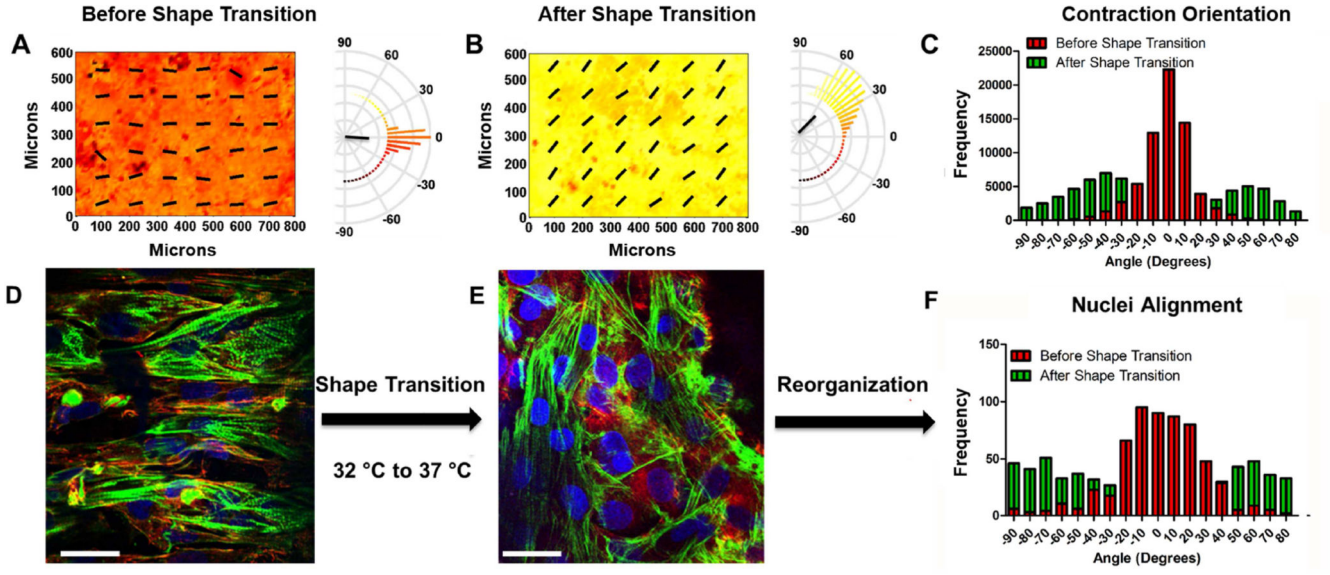

Figure 6. Alignment and contraction analysis of cardiac cell monolayer reorganization caused by an orthogonal shift in the orientation of PCL-based shape memory nanogrooves

The direction of contraction at each location in the heat map before (A) and after (B) shape transition is indicated by color [coded to the polar histograms] and the overlaid vector field. Semicircular histograms of contraction angles indicate the overall directionality of contracting cardiac cells, of one field of view, on surfaces before and after shape transition. The black lines in the center of the histogram indicate the mean resultant vector length. The shift in contraction direction is better visualized in (C). The distribution of the contraction orientation after shape transition exhibits a bimodal behavior and does not behave like a Gaussian distribution. (Kurtosis = 2.184, −1.220 before and after, respectively. *$p \leq 0.001$, n = 3, D'Agostino & Pearson omnibus normality test). Representative images of NRVM alignment on SMPs before (D) and after (E) shape transition (nuclei staining = blue, f-actin staining = green, vinculin staining= red; scale bar = 20 μm). Histograms of NRVM nuclei (F) before and after shape transition.

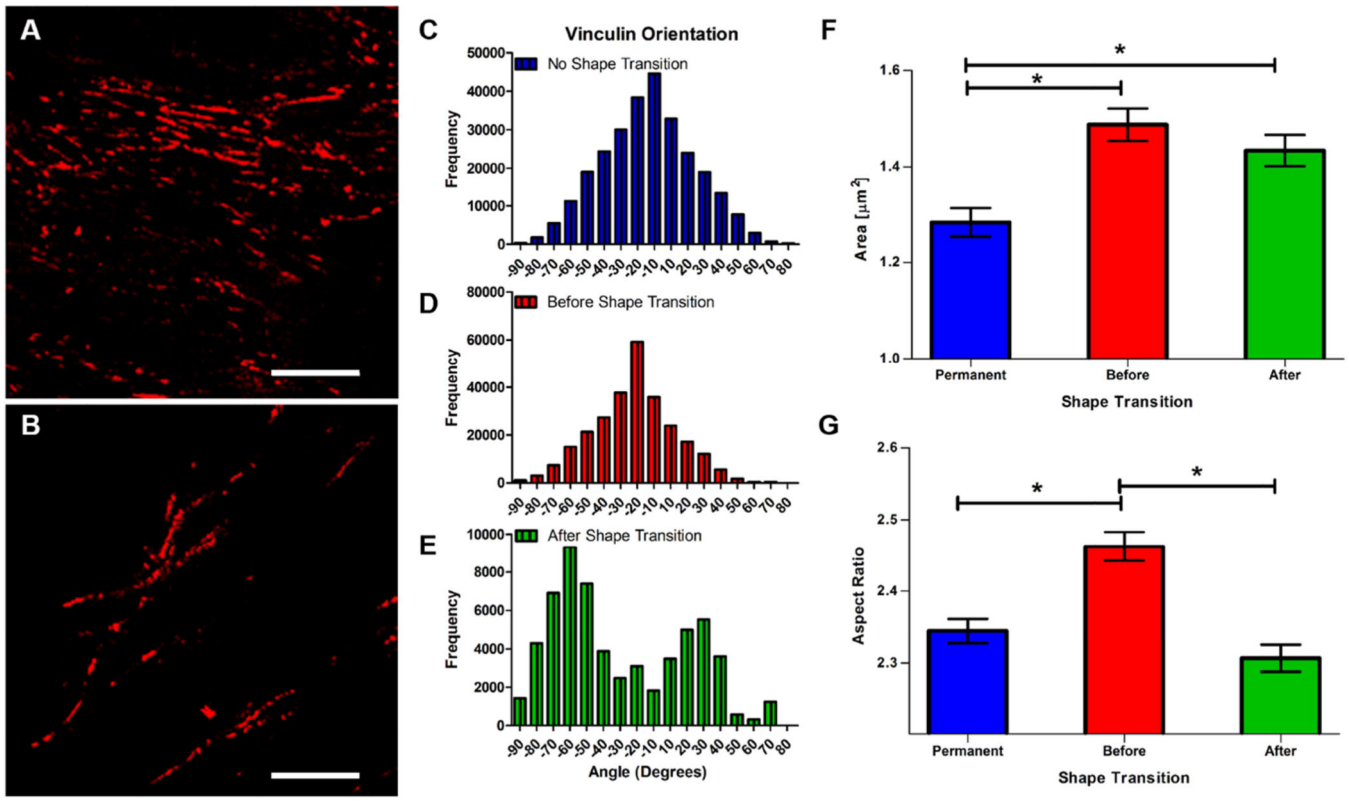

Figure 7. Effect of shape transition on cardiomyocyte vinculin orientation and shape

(A) Representative image of NRVMs on SMP substrates before (A) and after (B) shape transition stained for vinculin (red) (scale bar = 10μm). (C, D, and E) Vinculin orientation distribution on permanent and SMP substrates. (F) Area of vinculin staining on permanent (mean ± standard error mean = 1.28±0.030) and SMP substrates before (1.49 ± 0.034) and after (mean = 1.434 ± 0.032) shape transition (n=1000 for all conditions). (G) Aspect ratio of vinculin staining on permanent (2.35 ±0.017) and SMP substrates before (2.46 ± 0.020) and after (2.307 ± .019) shape transition (no shape transition, n = 2028; before shape transition, n=1997; after shape transition, n=1447; * = p-value<0.001; * = p-value<0.0001).